Granular flow in rotating cylinders with noncircular cross sections

D. V. N. Prasad and D. V. Khakhar*

Department of Chemical Engineering, Indian Institute of Technology—Bombay, Powai, Mumbai 400076, India

(Received 11 May 2007; revised manuscript received 18 December 2007; published 2 April 2008)

An experimental and theoretical study is carried out of the flow of granular material in cylinders with different cross-sectional shapes rotated about their axes. The flow of particles in such geometries is confined to a shallow layer at the free surface. The length and thickness of the layer shrink and expand periodically with rotation of the cylinder, resulting in chaotic advection and improved mixing of passive tracers. Experimental results obtained by flow visualization are reported for quasi-two-dimensional mixers half filled with glass beads. A depth-averaged flow model to predict the time-varying layer thickness profile is presented, along with a perturbation solution in terms of a small parameter k, which is the ratio of the maximum layer thickness to the half length of the layer (L), at the cross-section orientation when the length is minimum. To the lowest order [$O(k^0)$], the model predicts that the layer profiles scaled with $L(\theta)$ at different mixer orientation angles (θ) are identical and the same as that for a circle. The measured layer thickness profiles averaged over different orientations of noncircular mixers match reasonably well with the theory, but the standard deviations are larger for the noncircular cylinders compared to the circle. The $O(k)$ perturbation solution and the full theory both predict that the scaled layer thickness varies periodically; the deviations are proportional to the rate of change of the length with orientation. The perturbation solution gives results close to those from the numerical solution except at cylinder orientations when the length of the flowing layer changes sharply. The measured variation of the scaled midlayer thickness with orientation for all geometries is well predicted by the theory.

DOI: 10.1103/PhysRevE.77.041301 PACS number(s): 45.70.Mg, 83.80.Fg

I. INTRODUCTION

Rotating cylinders are commonly used in many industrial processes involving granular materials for operations such as mixing, drying, coating, and granulation [1]. With increasing rotational speed of the cylinder, different flow regimes—slipping, avalanching, rolling, cascading, cataracting, and centrifuging—are obtained [2,3]. The rolling flow regime is the most common mode of operation in industrial systems. The flowing material in this regime is confined to a shallow layer at the free surface and the rest of the material undergoes a solid body rotation as a fixed bed [4,5].

The length of the flowing layer changes with orientation of the mixer and thus the flow of granular particles in noncircular rotating cylinders is time periodic. The time-periodic flow leads to chaotic advection of particles, thereby improving the overall mixing efficiency in noncircular cross sections [6]. In segregating systems, different segregation patterns are obtained as a result of the balance between chaotic mixing and segregation [7,8].

Although the surface flow of granular materials in rotating circular cylinders has been studied theoretically [5,9–12] and experimentally [9,12–14], the flow in noncircular cross sections has not been investigated in any detail. Experiments in a rotating cylinder with square and elliptical cross sections rotated at low speeds indicate that the ratio of midlayer layer thickness to the length remains nearly unchanged with time [6]. This model has been used to describe cross-sectional mixing and segregation in cylinders with noncircular cross sections [6–8,15,16]. A similar approach has been used for analyzing mixing and segregation in circular cylinders but with a periodically varying rotational speed [17]. A more detailed understanding of the flow in noncircular geometries would be useful for a better description of mixing and segregation in such systems, which have the potential for practical application.

In this paper we make a study of the flow in cylinders with different noncircular cross sections at steady state by means of theory and experiment. The shapes of the time-varying flowing layer are studied experimentally by means of flow visualization in quasi-two-dimensional (2D) rotating cylinders. A theory is developed using depth-averaged mass and momentum balance equations and a perturbation solution is obtained. The paper is structured as follows. Experimental details are presented in the next section. The theory for flow in noncircular cylinders is given in Sec. III. Theoretical and experimental results and comparisons between the two are presented in Sec. IV. Conclusions of the work are summarized in Sec. V.

II. EXPERIMENTAL DETAILS

Experiments to determine the flowing layer profiles are carried out in quasi-two-dimensional cylinders with different cross-sectional shapes shown in Fig. 1—circle, square, star, and retrofitted circles with two and four triangular wedges pointing toward the axis and placed diametrically (referred to as W2 and W4 below). The length of the chord of the triangular inserts in W2 and W4 is $2l$ and the apex angle is 2λ. The star cross section may also be considered to be W4 with the circle diameter equal to the length of the largest diagonal. The parameters for these geometries are given in Table I. L_0, half the minimum free surface length, is also given in Table I for different geometries. The square, star, and W4 cross sections are rotationally symmetric to 90° rotations whereas

*khakhar@iitb.ac.in

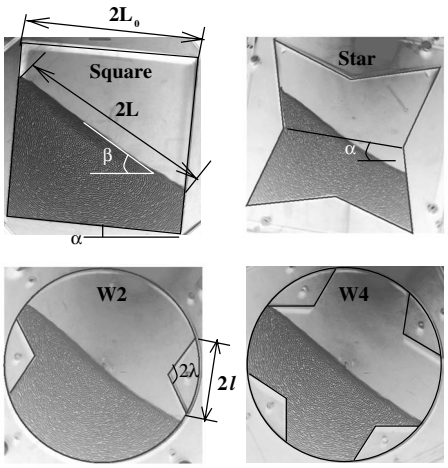

FIG. 1. Noncircular geometries used in the experiments. Geometrical features of the mixers are marked.

W2 is symmetric to 180° rotations. The thickness of the cylinder is 10 mm in all cases. The sidewalls of square cross section are made of aluminum, whereas other geometries have acrylic sidewalls. A glass plate is used on the front for good image quality. The back plate used is glass for the square and star. In the cases of the circle, W2, and W4, an acrylic back plate is used so as to facilitate attachment of the inserts by screws for W2 and W4. A computer-controlled stepper motor with a sufficiently small step is used to rotate the cylinder. 1 and 3 mm glass beads in a narrow size range (± 0.1 mm and ± 0.2 mm, respectively) are used in the experiments, and the cylinders are half filled with particles. Experiments are carried out at four different rotational speeds (2, 3, 4 and 5 rpm); the flow is in the rolling regime in all cases. The cylinder is rotated at the set speed for sufficiently long times to achieve a steady periodic motion before measurements are made. A digital camera (Nikon Coolpix 5000), focused on the flowing layer, is used to capture images while the cylinder is in rotation. Low shutter speeds (1/4–1/30 s) are used so that the interface between the flowing layer and the rotating bed is distinct. The procedure followed for analysis is similar to that of Orpe and Khakhar [13].

Around 25 images are captured at different orientations for W2 and W4 and around 60 images for the square and star cross sections. Ten images are captured for a circular cross section. A line is joined to the corners of the streak lines in each image, representing the interface between the flowing layer and the fixed bed, using an image analysis software (Image Pro Plus). Similarly, a line is drawn along the free surface. The traced lines comprise about 20 points each in a coordinate system with its origin at the cylinder. A sixth-degree polynomial is fitted to each of these outlines. The length of the flowing layer is obtained numerically from the free surface polynomial. The thickness of the flowing layer (δ) is obtained as the perpendicular distance from the bed-layer interface to the free surface as given by the fitted polynomials.

The absolute angle of orientation of each mixer, α, is taken to be the angle with the horizontal made by the line corresponding to the shortest length (Fig. 1). The range of angles is (0°,90°) for square, star, and W4 cross sections (as the symmetry in these geometries is with respect to every 90° rotation) and is (0°,180°) for W2. The dynamic angle of repose (β) is taken to be the angle of the free surface at the midpoint ($x=0$). This is obtained by calculating the derivative of the fitted polynomial curve of the free surface at $x=0$. An image is captured after stopping the rotation of the cylinder and the angle of the static free surface is taken to be the static angle of repose (β_s).

TABLE I. Geometric parameters for the different cylinders used.

Shape	L_0 (mm)	λ (deg)	l (mm)
Circle.	160.0.		
Square	141.5		
Star	119.0	73	165
W2	110.0	60	64
W4	110.0	60	64

III. THEORY

Consider the granular flow in a noncircular cylinder with the length of the flowing layer $[2L(t)]$ and the thickness of the flowing layer $[\delta(x,t)]$ varying with time (t) as the cylinder rotates. The cross-sectional shapes of the cylinder are limited to be those that are symmetric to 180° rotations, and the cylinder is half filled with granular material so that the free surface passes through the centroid of the cylinder at all times. This results in simplification of the calculation of the free surface length.

The depth-averaged mass and momentum balance equations for the flow in the layer are [9,13]

$$\frac{\partial \delta}{\partial t} + \frac{\partial (u\delta)}{\partial x} = -\omega x, \tag{1}$$

$$\frac{\partial (u\delta)}{\partial t} + \frac{4}{3}\frac{\partial (u^2\delta)}{\partial x} = g\delta A - 4cd\frac{u^2}{\delta}, \tag{2}$$

where u is the mean velocity in the layer, d is the particle diameter, g is the acceleration due to gravity, and $A=\sin(\beta-\beta_s)/\cos\beta_s$. $c\approx 1.5$, the collisional viscosity constant, and β_s, the static angle of repose, are model parameters. The above equations are obtained assuming a linear velocity profile, a constant bulk density in the layer and bed, and a specific form of the shear stress at the base of the layer comprising frictional and collisional components [9,13]. In Eq. (2) the first term on the right-hand side is the gravitational driving force less the frictional resistance, while the second term gives the viscous term arising from collisional momentum transfer. Equations (1) and (2) do not have a time-periodic driving term, and the time periodicity of the flow results from the boundary conditions, which depend on the mixer orientation.

The layer thickness is much smaller than its length, and we define a small parameter k, which is of the order of the

ratio of the maximum layer thickness to the length of the layer. Using this parameter, we obtain the following dimensionless variables, which are used to rescale the governing equations: $\eta = x/L(\theta)$, $\theta = \omega t$, $\phi = \delta/kL(\theta)$, and $U = uk/\omega L(\theta)$, where ω is the cylinder rotational speed. The rescaled mass balance equation [Eq. (1)] is

$$k\frac{\partial \phi}{\partial \theta} + \frac{\partial (U\phi)}{\partial \eta} = -\eta - k\phi f, \tag{3}$$

where $f(\theta) = (1/L)dL/d\theta$ is a known function determined by the mixer shape. Noncircular cross sections, which have $f \neq 0$, thus result in an additional source term in the mass balance equation. Similarly, the rescaled momentum balance equation is

$$k\frac{\partial (U\phi)}{\partial \theta} + \frac{4}{3}\frac{\partial (U^2\phi)}{\partial \eta} = \frac{\phi}{\bar{L}\,\mathrm{Fr}} - \frac{4sU^2}{\phi \bar{L}} - 2kU\phi f, \tag{4}$$

where $\bar{L} = L/L_0$, $L_0 = L(0)$, and the dimensionless parameters are the modified Froude number $\mathrm{Fr} = \omega^2 L_0/gk^2A$ and the modified size ratio $s = cd/k^2L_0$. Again, the structure of the momentum balance equation is preserved but with an additional source term due to the changing free surface length. The boundary conditions for the above equations are time independent.

We consider the case of low rotational speeds when $\mathrm{Fr} = O(k)$ or smaller, for which Eq. (4) reduces to

$$\frac{\phi}{\bar{L}\,\mathrm{Fr}} - \frac{4sU^2}{\phi \bar{L}} = 0, \tag{5}$$

since $s = 1/\mathrm{Fr}$ as shown below. The dimensionless shear rate is then

$$\frac{2U}{\phi} = (s\,\mathrm{Fr})^{-1/2}, \tag{6}$$

and the shear rate is given by

$$\dot{\gamma} = \frac{2u}{\delta} = (gA/cd)^{1/2}. \tag{7}$$

Thus, in this limit, the shear rate is a constant, as found earlier for a circular cylinder [18]. Further, taking $k = (\omega/\dot{\gamma})^{1/2}$ and using Eq. (7) and the definitions of Fr and s, we obtain $s\,\mathrm{Fr} = 1$. Equation (6) then yields the dimensionless mean velocity in the layer as $U = \phi/2$. Using this result, the rescaled continuity equation [Eq. (3)] reduces to

$$k\frac{\partial \phi}{\partial \theta} + \frac{1}{2}\frac{\partial (\phi^2)}{\partial \eta} = -\eta - k\phi f. \tag{8}$$

The layer thickness must vanish at the ends of the layer so that we can use $\phi = 0$ at $\eta = -1$ or $\phi = 0$ at $\eta = 1$.

Although it is not obvious from Eq. (8), the layer profile obtained from the equation is symmetric. The physical reasoning is as follows. The flow is in the positive η direction throughout the layer. Material enters the layer in the portion $\eta < 0$ and leaves the layer in the portion $\eta > 0$. Referring to Eq. (8), if $f > 0$ then the term $k\phi f$ results in a lower flux into the layer for $\eta < 0$ and a higher flux out of the layer for $\eta > 0$. Both result in a lower layer thickness and hence have a symmetric effect on the layer thickness. Similar arguments can be made for $f < 0$ and for the term $k\partial\phi/\partial\theta$ to show that the layer shape is symmetric. This can also be seen from the following derivation. Considering $\eta < 0$, we have upon integration of Eq. (8)

$$\phi^2 = (1 - \eta^2) - kf\int_{-1}^{-\eta} \phi\, d\eta - k\frac{\partial}{\partial \theta}\int_{-1}^{-\eta} \phi\, d\eta, \tag{9}$$

using the boundary condition $\phi = 0$ at $\eta = -1$. Similarly, for $\eta > 0$ we have

$$\phi^2 = (1 - \eta^2) - kf\int_{\eta}^{1} \phi\, d\eta - k\frac{\partial}{\partial \theta}\int_{\eta}^{1} \phi\, d\eta, \tag{10}$$

using the boundary condition $\phi = 0$ at $\eta = 1$. Putting $\eta = -\eta$ in Eq. (9), we obtain Eq. (10), indicating that the layer thickness profile is symmetric.

We consider next the long-time periodic solution of Eq. (8) for the noncircular cylinder shapes, when the transients of startup have decayed. Simulation of Eqs. (3) and (4) for a circular cylinder indicate that transients decay rapidly—typically within about 0.02 revolutions of the cylinder (see Fig. 8 of [19]). The characteristic time for decay of transients is thus $\tau_d = 1/\dot{\gamma}$, while that for change in the free surface length due to mixer rotation is $\tau_L = 1/\omega$. The ratio of the two is given by $\tau_d/\tau_L = k^2$, which is very small and hence transient flows may be neglected. A perturbation solution of the rescaled mass balance equation of the form

$$\phi(\eta, \theta) = \phi_0(\eta, \theta) + k\phi_1(\eta, \theta) + \cdots \tag{11}$$

is considered for the case when k is small. Upon substituting in Eq. (8) and collecting terms of the same order, we obtain

$$\frac{1}{2}\frac{\partial (\phi_0^2)}{\partial \eta} = -\eta, \tag{12}$$

to order k^0 $[O(k^0)]$ and

$$\frac{\partial \phi_0}{\partial \theta} + \frac{\partial (\phi_0\phi_1)}{\partial \eta} = \phi_0 f. \tag{13}$$

to $O(k^1)$. The boundary conditions are $\phi_0 = 0$ and $\phi_1 = 0$ at $\eta = -1$.

Solving Eq. (12), we obtain the layer thickness profile to lowest order as

$$\phi_0 = (1 - \eta^2)^{1/2}. \tag{14}$$

Equation (14) implies that to $O(k^0)$ the scaled layer profile is independent of orientation and the same as that for a circle. Further, the layer shape maintains geometrical similarity upon rotation of the mixer as found experimentally [6]. Substituting for ϕ_0 into Eq. (13), we obtain

$$\frac{\partial (\phi_0\phi_1)}{\partial \eta} = -\phi_0 f, \tag{15}$$

which upon integration yields

$$\phi_1 = -\frac{f}{\phi_0}\int_{-1}^{\eta} \phi_0 d\eta. \tag{16}$$

Since ϕ_0 is symmetric about $\eta=0$ it is straightforward to show that

$$\int_{-1}^{\eta} \phi_0 d\eta = \int_{-\eta}^{1} \phi_0 d\eta, \tag{17}$$

which implies that $\phi_1(\eta,\theta)=\phi_1(-\eta,\theta)$ and that the layer profile from the perturbation solution is also symmetric. Further, ϕ_1 vanishes at both ends of the layer as can be seen from the following derivation using l'Hospital's rule

$$\lim_{\eta\to-1}\frac{1}{\phi_0}\int_{-1}^{\eta}\phi_0 d\eta = \lim_{\eta\to-1}\frac{\phi_0}{d\phi_0/d\eta} = \lim_{\eta\to-1} -\frac{(1-\eta^2)}{\eta} = 0. \tag{18}$$

Thus the solution obtained is reasonable and the layer shape profile is qualitatively similar to that for a circular cylinder.

Upon integrating Eq. (16) and combining with Eqs. (11) and (14), we obtain the layer thickness profile as

$$\phi(\eta,\theta) = (1-\eta^2)^{1/2} - kf(\theta)\left(\frac{\cos^{-1}|\eta|}{2\phi_0} - \frac{|\eta|}{2}\right). \tag{19}$$

The variation of the midlayer thickness with time is then

$$\phi(0,\theta) = 1 - kf(\theta)\frac{\pi}{4}. \tag{20}$$

Now $\phi(0,0)=1-kf(0)\pi/4\approx 1$. This gives $\delta(0,0)/kL_0=1$ so that $k=\delta(0,0)/L_0$. Thus k is the scaled midlayer thickness at the orientation when the length of the flowing layer is minimum. We take k to be an input parameter for the model.

Assuming the free surface to be nearly flat, the length of the flowing layer is a geometric property and can be obtained in terms of the cylinder orientation angle for each cross section using the following equations.

For the square,

$$L = \begin{cases} \dfrac{L_0}{\cos\theta_m} & \text{if } \theta_m < \pi/4, \\ \dfrac{L_0}{\sin\theta_m} & \text{otherwise.} \end{cases} \tag{21}$$

For the star,

$$L = \begin{cases} \dfrac{L_0}{\cos\theta_m}\dfrac{\tan\lambda}{(\tan\lambda-\tan\theta_m)} & \text{if } \theta_m < \theta_d, \\ \dfrac{L_0}{\sin\theta_m}\dfrac{\tan\lambda}{(\tan\lambda-1/\tan\theta_m)} & \text{otherwise.} \end{cases} \tag{22}$$

For W2 and W4,

$$L = \begin{cases} \dfrac{(\sqrt{R^2-l^2}\tan\lambda - l)}{R\cos\theta_m(\tan\lambda-\tan\theta_m)} & \text{if } \theta_m < \theta_d, \\ R & \text{otherwise.} \end{cases} \tag{23}$$

In the above equations, $\theta_m=\theta \bmod(\pi/2)$ for the square, star, and W4 and $\theta_m=\theta \bmod(\pi)$ for W2. $\theta=(\alpha-\beta)$ is the difference between the absolute orientation angle α and the angle of repose β. In the star cross section, $\theta_d=\tan^{-1}[l/(L_0+l/\tan\lambda)]$ whereas $\theta_d=\sin^{-1}(l/R)$ in the case of W2 and W4 cross sections. R is the radius of the circle.

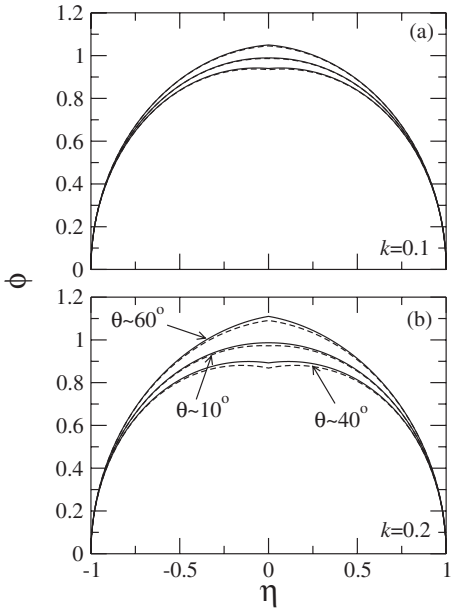

FIG. 2. Comparison of the scaled layer thickness profiles $[\phi(\eta,\theta)]$ obtained from the full model (solid lines) and the $O(k)$ theory (dashed lines) for different mixer orientations (θ) and k.

A finite-difference method (forward time, backward space) is used to numerically solve the equation of the full model [Eq. (8)]. Only half the layer is considered ($\eta<0$), taking advantage of the symmetry of the problem. A sufficiently small time step ($d\theta=1\times10^{-4}$) and distance interval ($d\eta=1.67\times10^{-3}$) are used. We compare our experimental results with both theory [Eq. (19)] and computations [Eq. (8)]. The code for numerical solution was validated by solving Eq. (8) numerically for a circular cylinder ($f=0$) and comparing with the exact solution ($\phi=(1-\eta^2)^{1/2}$).

IV. RESULTS AND DISCUSSION

A comparison of the layer thickness profiles obtained from numerical solution of the full model [Eq. (8)] and the $O(k)$ theory [Eq. (19)] are shown in Fig. 2 for a square. Results are shown for two values of k (0.1 and 0.2) which roughly span the range of the parameter values for the systems studied [$k\in(0.09,0.16)$]. The agreement between the $O(k)$ theory and full model results is reasonably good even for a relatively large value of k [$k=0.2$, Fig. 2(b)], although the agreement is better for $k=0.1$ [Fig. 2(a)]. The deviation is the largest at $\eta=0$, and we compare the variation of the midlayer thickness $[\phi(0,\theta)]$ with orientation as predicted by the full model and the $O(k)$ theory in Fig. 3 for both large and normal values of k. Although there is a good agreement between the $O(k)$ theory and the full model for most cross-section orientation angles, there is a significant deviation when the free surface is close to the corner of the square ($\theta=45°$), where there is a discontinuity in f. Also, the devia-

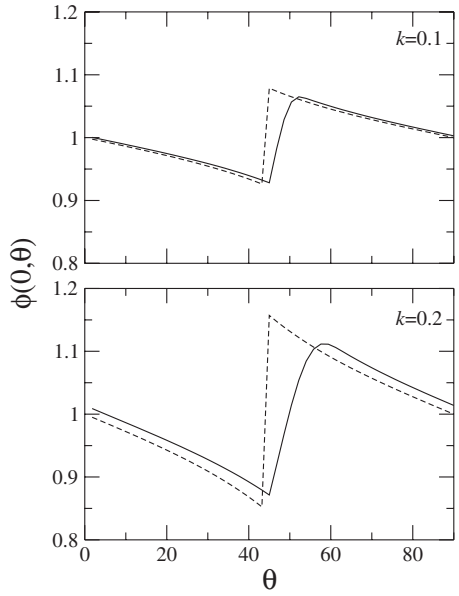

FIG. 3. Comparison of the scaled midlayer thickness $[\phi(0,\theta)]$ variation with mixer orientation (θ) obtained from the full model (solid lines) and the $O(k)$ theory (dashed lines) for different k.

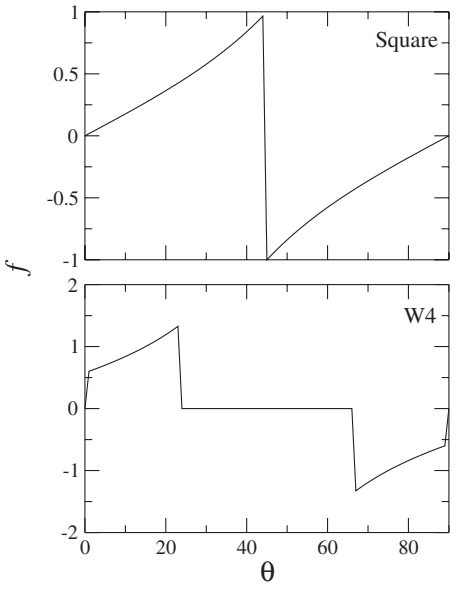

FIG. 4. Variation of the specific rate of change of free surface length with orientation $[f=(1/L)dL/d\theta]$ with mixer orientation (θ) in square and W4 cross sections.

tion increases with increase in k. The deviation occurs because $f\phi > 1/k$ for large values of $dL/d\theta$ and the perturbation solution is no longer valid.

The scaled midlayer thickness varies in three different phases: a slow decrease for $\theta=0°-45°$, a rapid increase between 45° and 60°, and a slow decrease between 60° and 90°. The different phases observed in the experiments can be explained using Eq. (8). When θ is between 0° and 45°, $dL/d\theta$ is positive and its magnitude increases as it approaches the corner of the mixer (where the length of the layer is maximum). As a result, the time-dependent driving term in Eq. (8) is negative (Fig. 4) and the scaled midlayer thickness decreases monotonically. When the corner of the cylinder is reached, the driving term in Eq. (8) changes sign, resulting in a sharp increase in the scaled midlayer thickness. In the final phase where $dL/d\theta$ is negative, the source term in Eq. (8) is positive but reduces in magnitude with rotation. Thus the scaled midlayer thickness decreases.

Figure 4 shows the variation of f with θ in the square and W4 cross sections. A sharp change in f at $\theta=45°$ can be seen in the square, whereas is it discontinuous at three different orientation angles in W4. The variation for the star cross section is similar to that in a square but with an additional discontinuity at $\theta=0$. The variation for W2 is very similar to that for W4 but with $f=0$ between $\theta=24°$ and 156°.

Figure 5 shows the experimental surface layer profiles for 3 mm particles rotated in a square at 3 rpm at four different orientations. The absolute orientation angle α, the free surface angle β, and the mixer orientation θ are shown in the figure. At $\alpha \approx 39°$, $\theta \approx 0$, and the length is minimum. As θ increases, the length of the free surface increases. The maximum length of the layer is obtained when θ is near 45°, which in this case occurs when the orientation angle is close to 86°. The length of the flowing layer shrinks upon further increase of θ.

Figure 6 shows the scaled flowing layer shapes at two different orientation angles for different noncircular cross-sections rotated at 5 rpm. The cylinder boundaries are not shown in this figure for clarity. As can be seen, the thickness of the flowing layer and the free surface angle change with orientation angle of the mixer. The layer profiles in noncircular cylinders are qualitatively similar to those in a circular cross section [13]. Experimental measurements indicate that the layer surface becomes curved at high rotational speeds and the curvature is greater for 1 mm particles than 3 mm particles, as found previously for circular cylinders [13].

The scaled layer thickness profiles, $\delta/L=k\phi$, for 3 mm glass beads in various geometries for three different rotational speeds are shown in Fig. 7. The points are averages of profiles measured at different orientations in noncircular mixers and the error bars indicate the standard deviation from the average value. With the increase in rotational speed, the scaled thickness of the layer increases for all cross sections. The profiles are nearly symmetric for all cases, particularly at lower speeds. For a particular rotational speed, the midlayer thickness in noncircular cross sections is greater than that in the circular cross section. The layer thickness profiles $(\delta/L=k\phi_0)$ obtained from the $O(k^0)$ theory [Eq. (14)] are shown as solid lines in the figure. The fitted values of k, taken to be the ratio of the experimentally measured midlayer thickness to the length of the flowing layer at $\theta=0$, are indicated in the figure. The predictions of Eq. (14) match reasonably well with the scaled experimental layer thickness profiles. The results for 1 mm particles are similar.

The size of the error bars in Fig. 7 gives an indication of the error of the measurement in circular cylinders, whereas it indicates the accuracy of the scaling, in addition to the error, for the noncircular cross sections. The results for the circle indicate that the error in measurement is small. For the noncircular cross sections the results show that the scaling is

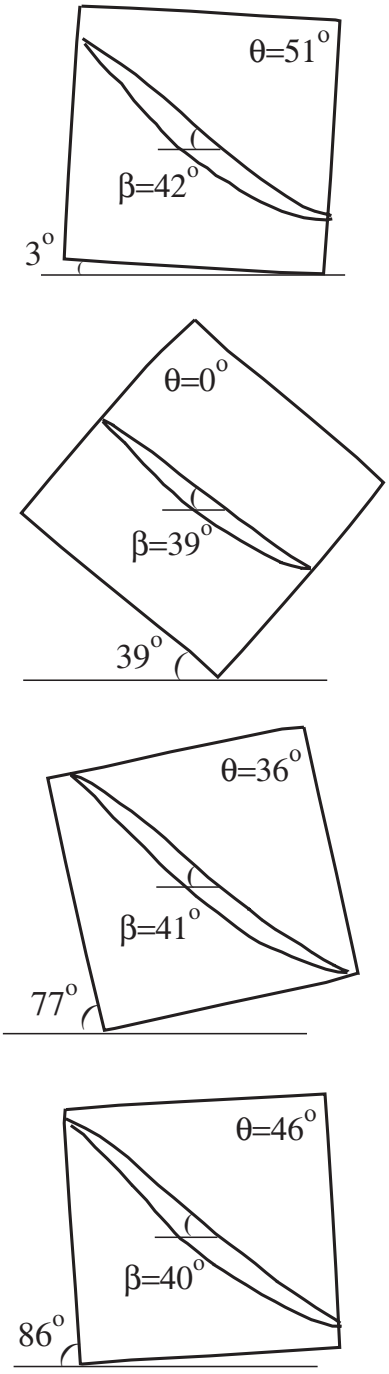

FIG. 5. Variation of the flowing layer for 3 mm particles rotated in a square geometry at 3 rpm at different orientations. The relative orientation $\theta=(\alpha-\beta)$, the difference between the orientation angle α and the free surface angle β is also indicated for each case.

quite good at lower rotational speeds (deviation of about one particle diameter) and becomes increasingly inaccurate at higher speeds (deviation up to three particle diameters). The deviations for the star, W2, and W4 cross sections are larger as compared to those for the square. The error bars give the average deviation from the mean over all orientations; however, the error may be larger at some orientations, as shown below.

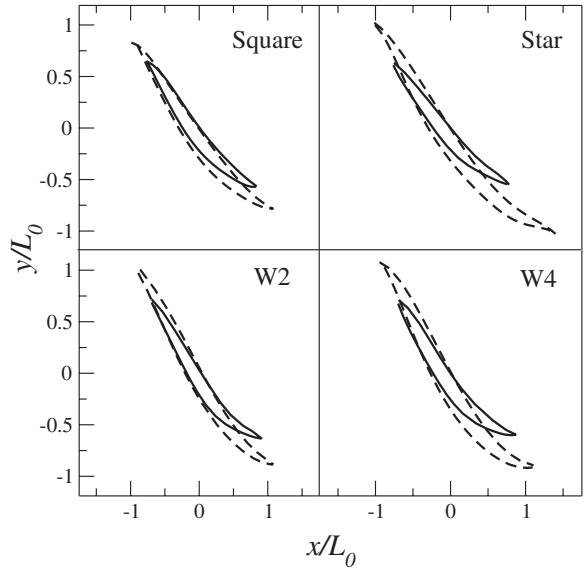

FIG. 6. Experimentally obtained flowing layer shapes for 3 mm particles rotated in different noncircular cross sections at 5 rpm. Solid lines are for mixer orientation $\theta\approx 0°$ and dashed lines are for $\theta\approx 45°$.

The dynamic angle of repose β varies with the orientation angle α of the mixer and is shown in Fig. 8 for 3 mm glass beads. At the lowest rotational speed (2 rpm), the variation of β is small in all cases. At higher rotational speeds, the angle of repose decreases initially and after reaching a minimum value, it again increases. The variation is similar to that of the length L with orientation, and both β and L have minima

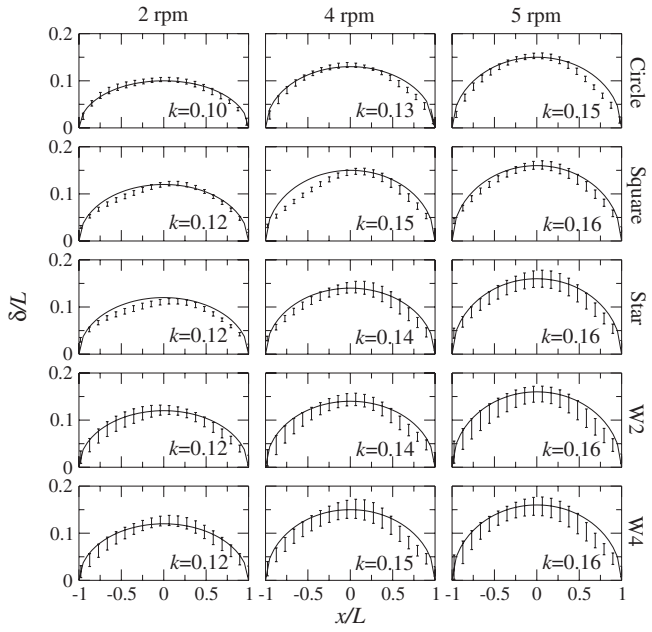

FIG. 7. Comparison of measured layer thickness profiles scaled with length, $L(\theta)$ for 3 mm glass beads at different rotational speeds in various cylinder cross sections (points with error bars) with the $O(k^0)$ theory [Eq. (14)] (solid line). The experimentally obtained value of k is shown in each case.

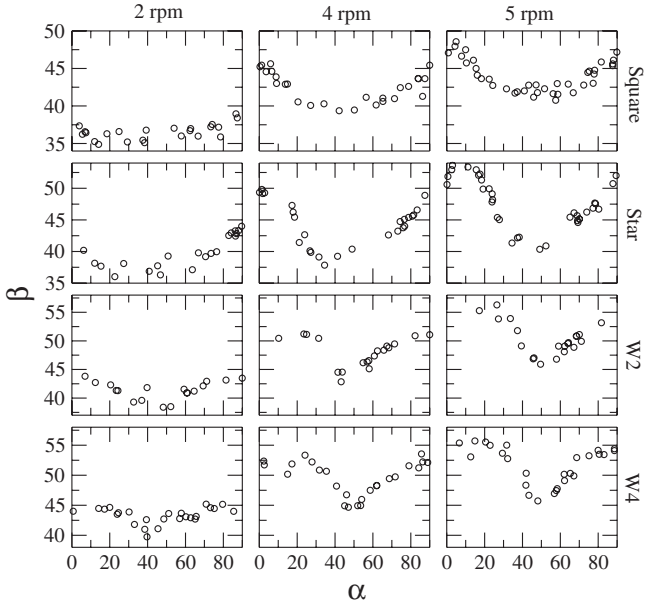

FIG. 8. Variation of the angle of repose β with orientation angle α for 3 mm particles in various mixer cross sections rotated at different rotational speeds.

and maxima at the same angles (Fig. 9). In W2 and W4, the angle of repose is nearly constant at times when the length of the flowing layer is constant. In W2, the variation of β for $\alpha > 90°$ is a mirror image of its variation for $\alpha < 90°$ and is not shown in the figure. A qualitatively similar trend is obtained for 1 mm glass beads.

The length of the flowing layer in each cross section can be calculated using Eqs. (21)–(23). In our calculations, we approximate β to be β_0 (surface angle when the free surface length is minimum). Figure 9 shows comparison of the measured and calculated lengths of the free surface for 3 mm glass beads in various cylinder cross sections at three different rotational speeds. Symbols are experimental results and solid lines represent calculations using Eqs. (21)–(23), depending on the cross section. The match is very good for all geometries with the approximation of $\beta = \beta_0$ in the above equations. A similar match is found for experimental data for 1 mm glass beads. Thus variation in the surface angle during rotation does not significantly affect the length. We use this approximation in theoretical calculations given below.

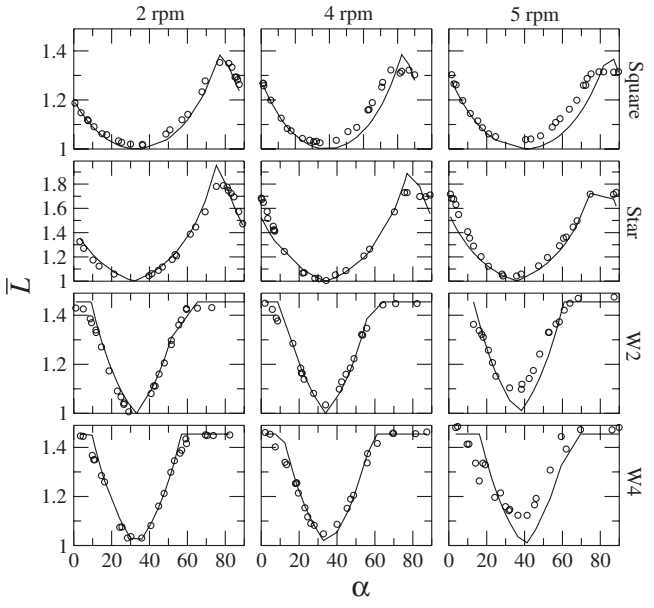

FIG. 9. Comparison of experimental values of $\bar{L}$ for 3 mm particles in various mixer cross sections rotated at different rotational speeds (symbols) with calculated lengths using Eqs. (21)–(23) with $\beta = \beta_0$ (solid lines).

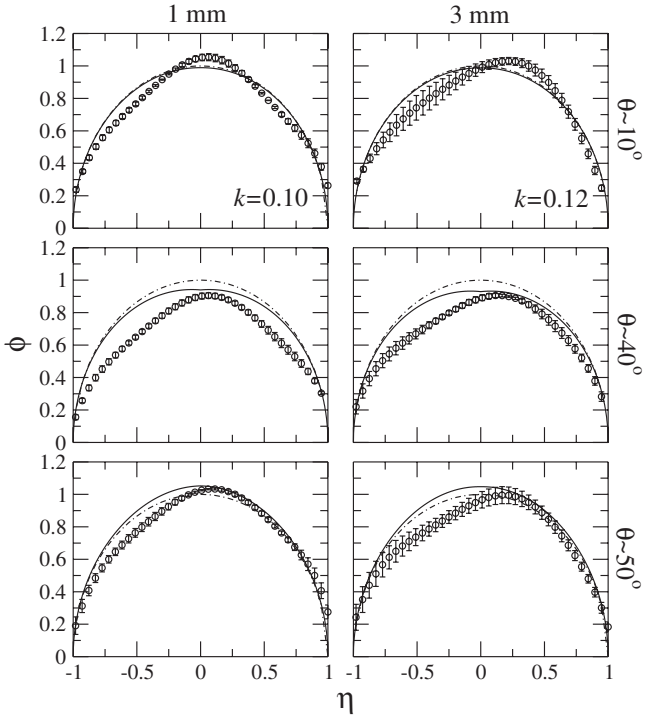

FIG. 10. Comparison of the scaled experimental layer thickness profiles $[\phi(\eta, \theta)]$ for 1 mm (left column) and 3 mm (right column) glass beads at three different orientations of a square mixer rotated at 2 rpm (symbols with error bars) with $O(k)$ theory (dashed line), $O(k^0)$ theory (dot-dashed line), and computations (solid line). The value of k is indicated in each case.

Scaled layer thickness profiles measured at different orientations are shown in Fig. 10 for 1 and 3 mm particles in a square cross section rotated at 2 rpm. The error bars indicate the standard deviation over at least three measurements. The error bars are smaller as compared to those in Fig. 7 since the averaging is over a narrow range of orientation angles in each case ($\pm 2°$). The orientation angle $\theta = 10°$ corresponds to a low value of the rate of change of length ($dL/d\theta$), whereas this value is large at $\theta = 40°$ and 50°. The results indicate that the midlayer thickness and the layer shape profile change with orientation. The figure also shows the predictions of the full model and the $O(k^0)$ theory. The experimental profiles have a sharper peak and are skewed compared to the predicted profiles. The full model gives marginally better predictions than the $O(k^0)$ model, but there are deviations in this case as well. The deviations are of the

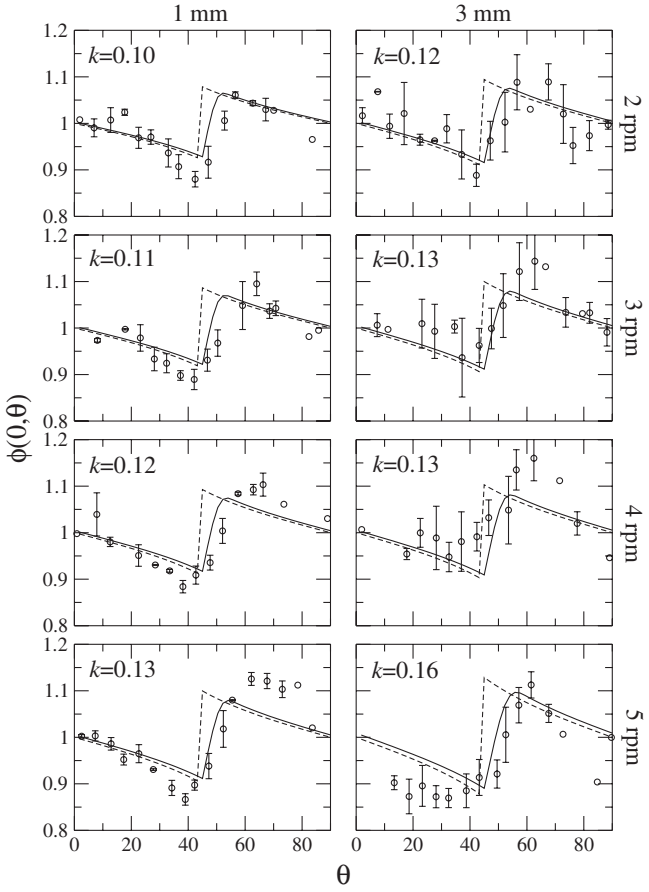

FIG. 11. Variation of scaled midlayer thickness $[\phi(0,\theta)]$ in a square cross section with orientation (θ) at different rotational speeds. Symbols with error bars represent experimental data averaged over every 5° rotation for 1 (left column) and 3 (right column) mm glass beads. Solid lines are results from numerical solution of the full model and dashed lines are predictions of the $O(k)$ theory. The value of k is indicated in each case.

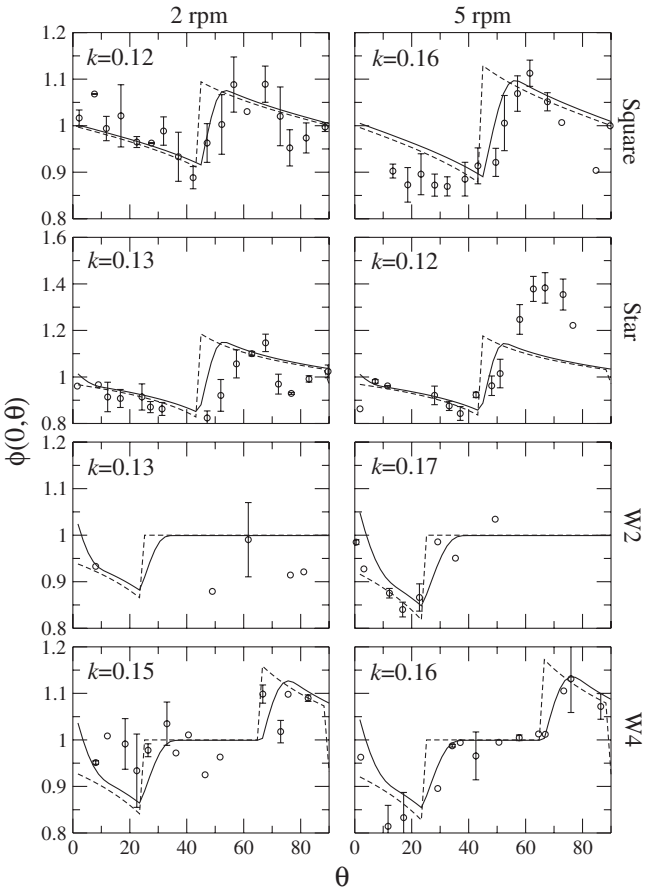

FIG. 12. Variation of scaled midlayer thickness $[\phi(0,\theta)]$ with orientation (θ) in different cylinder cross sections rotated at 2 (left column) and 5 (right column) rpm. Symbols with error bars represent experimental data for 3 mm glass beads averaged over every 5° rotation. Solid lines are results from numerical solution of the full model and dashed lines are predictions of the $O(k)$ theory. The value of k is indicated in each case.

order of one particle diameter and were noted in [13] for circular cylinders. Similar results are obtained at higher rotational speeds and for the other cross sections.

A more detailed comparison between experimental results and theory is considered in terms of the scaled midlayer thickness $[\phi(0,\theta)]$. The variation of the measured midlayer thickness with time for 1 and 3 mm glass beads in a square cross section at different rotational speeds is shown in Fig. 11. The average midlayer thickness and the corresponding standard deviation are calculated over every 5° rotation of the mixer. The error bars indicate the standard deviation from the average value in the figure. The error bars are larger in the experiments carried out with 3 mm glass beads as compared to the 1 mm particles. Predictions of the $O(k)$ model [Eq. (20)] and computational results from the full model [Eq. (8)] are also shown in Fig. 11. The computational results from the full model are close to the experimental results in all three phases discussed earlier. The perturbation theory gives good predictions everywhere except near the corners of the square, where a discontinuous change in f occurs. Note that the $O(k^0)$ theory yields a constant value of the scaled midlayer thickness $[\phi_0(0,\theta)=1]$.

The variation of the scaled midlayer thickness with orientation for the different cross sections is shown in Fig. 12 for 3 mm particles and two rotational speeds. The orientation angles at which only single values are available are shown as symbols without error bars in the figure. The qualitative trend of variation of midlayer thickness is the same in both square and star cross sections. In W2 and W4 geometries, when $dL/d\theta=0$, the layer thickness is constant. The variation of midlayer thickness in W2 for $\theta>90°$ is similar to that for W4 for $\theta>45°$. Results of the full model and the $O(k)$ solution are also shown in the figure. The predictions of Eq. (8) (full model) are once again closer to experimental values as compared to those of Eq. (20) [$O(k)$ solution] in all the cylinder cross sections at 2 rpm. At the highest rotational speed (5 rpm), the match between experiments and theory is good for W2 and W4. The deviations between model and experimental values in the square and the star cross sections are relatively higher at a few orientations of the mixer.

V. CONCLUSIONS

We presented a detailed study of the granular surface flow in rotating cylinders with different cross-sectional shapes.

The effects of particle size and rotational speed in each of the cylinder cross sections were considered. The length and thickness of the flowing layer change with orientation in noncircular cross sections. The free surface becomes curved at high rotational speeds and the curvature is greater for particles of smaller size. The shape of the layer in noncircular cross sections is similar to that in a circle. The thickness of the layer increases with particle size and rotational speed of the cylinder. The thickness of the layer is higher for noncircular cylinders than for a circular mixer.

The free surface angle (β) also changes periodically in noncircular cross sections. The change of β with orientation has a similar qualitative trend as the length, $L(\theta)$—both have minima and maxima at the same orientations. The layer length at any orientation depends on $\theta=(\alpha-\beta)$ and is determined by the geometry of the cylinder. The length of the layer is not sensitive to variations in the surface angle (β), and computations using the value of β at the orientation when the length is minimum (β_0) gave good predictions of the layer length.

A model based on the depth-averaged mass and momentum balance equations in the limit of low Froude numbers is obtained for the flow in noncircular cylinders. The shear rate in this limit is shown to be constant. The model predicts a symmetric layer thickness profile for all cases. A perturbation solution is obtained by considering an expansion in terms of the small parameter $k=\delta(0,0)/L(0)$. The perturbation solution is in reasonable agreement with the numerical solution of the full model at all orientations except near corners of the geometry, when there is a discontinuous change in $dL/d\theta$. The perturbation solution to $O(k^0)$ indicates that the layer thickness profiles scaled with $L(t)$ are the same at different cylinder orientations. This is in agreement with the model proposed by Khakhar *et al.* [6]. To $O(k)$ the theory indicates that the changing layer length results in an additional source term which produces a periodically varying scaled layer thickness. For orientations where the length is increasing ($dL/d\theta>0$), the source term is negative, resulting in a lower scaled thickness, and for orientations for which $dL/d\theta<0$, the reverse is true.

The measured layer thickness profiles scaled by $L(\theta)$ and averaged over different orientations of noncircular cylinders are close to those predicted by the $O(k^0)$ model at low rotational speeds. However, at high rotational speeds large error bars are obtained, indicating inaccuracy of the scaling. The layer thickness and the profile shapes change with orientation and the full theory gives better predictions than the $O(k^0)$ theory. However, the experimental layer thickness profiles are more sharply peaked and slightly skewed compared to the model predictions.

Detailed comparisons of the measured midlayer thickness and predictions of the full model and perturbation solution are presented. The variation of the scaled midlayer thickness about $\phi=1$, which corresponds to the $O(k^0)$ model, is significant [$\pm 10\%$ about the $O(k^0)$ value]. The full model gives good predictions for all geometries, particularly at low rotational speeds. The results indicate that deviations from the $O(k^0)$ model [$\phi_0(0,\theta)=1$] are maximum at orientations of the mixer at which there is a large change in $dL/d\theta$, that is, when the free surface crosses corners. Such sharp changes in the layer thickness may have an impact on mixing patterns.

[1] R. H. Perry and D. W. Green, *Perry's Chemical Engineers' Handbook* (McGraw Hill, New York, 1984).
[2] H. Henein, J. K. Brimacombe, and A. P. Watkinson, Metall. Trans. B **14**, 191 (1983).
[3] J. Mellmann, Powder Technol. **118**, 251 (2001).
[4] J. Rajchenbach, Phys. Rev. Lett. **65**, 2221 (1990).
[5] S. J. Rao, S. K. Bhatia, and D. V. Khakhar, Powder Technol. **67**, 153 (1991).
[6] D. V. Khakhar, J. J. McCarthy, J. F. Gilchrist, and J. M. Ottino, Chaos **9**, 195 (1999).
[7] K. M. Hill, D. V. Khakhar, J. F. Gilchrist, J. J. McCarthy, and J. M. Ottino, Proc. Natl. Acad. Sci. U.S.A. **96**, 11701 (1999).
[8] K. M. Hill, J. F. Gilchrist, J. M. Ottino, D. V. Khakhar, and J. J. McCarthy, Int. J. Bifurcat. Chaos Appl. Sci. Eng. **9**, 1467 (1999).
[9] D. V. Khakhar, J. J. McCarthy, T. Shinbrot, and J. M. Ottino, Phys. Fluids **9**, 31 (1997).
[10] T. Elperin and A. Vikhansky, Europhys. Lett. **42**, 619 (1998).
[11] H. A. Makse, Phys. Rev. Lett. **83**, 3186 (1999).
[12] Y. L. Ding, J. P. K. Seville, R. Forster, and D. J. Parker, Chem. Eng. Sci. **56**, 1769 (2001).
[13] A. V. Orpe and D. V. Khakhar, Phys. Rev. E **64**, 031302 (2001).
[14] A. A. Boateng and P. V. Barr, J. Fluid Mech. **330**, 233 (1997).
[15] S. E. Cisar, P. B. Umbanhowar, and J. M. Ottino, Phys. Rev. E **74**, 051305 (2006).
[16] S. W. Meier, S. E. Cisar, R. M. Lueptow, and J. M. Ottino, Phys. Rev. E **74**, 031310 (2006).
[17] S. J. Fiedor and J. M. Ottino, J. Fluid Mech. **533**, 223 (2005).
[18] D. V. Khakhar, A. V. Orpe, and J. M. Ottino, Adv. Complex Syst. **4**, 407 (2001).
[19] D. V. Khakhar, A. V. Orpe, and J. M. Ottino, Powder Technol. **116**, 232 (2001).